Production Engineering (2019) 13:211–217
https://doi.org/10.1007/s11740-018-0863-7

PRODUCTION PROCESS

Extent of embossing-related residual stress on the magnetic properties evaluated using neutron grating interferometry and single sheet test

Simon Vogt[1] · Tobias Neuwirth[2] · Benedikt Schauerte[3] · Hannes Alois Weiss[1] · Peter Markus Falger[1] · Alex Gustschin[4] · Michael Schulz[2] · Kay Hameyer[3] · Wolfram Volk[1]

Received: 2 August 2018 / Accepted: 30 November 2018 / Published online: 12 December 2018
© German Academic Society for Production Engineering (WGP) 2018

Abstract
Due to the permanently increasing maximum speed of modern electric machines, the mechanical load on the electrical steel rises. The punched flux barriers of reluctance machines play an increasingly key role in the mechanical design. The weakening of the material and the notching effect can cause local failure due to centrifugal force. In this paper, a method is presented which induces residual stresses by embossing electrical steel laminations, which contribute to the guidance of the magnetic flux and cause a negligible mechanical weakening of the sheet. The aim of this paper is to demonstrate the effectiveness of these embossed flux barriers. This is achieved by using neutron grating interferometry, that allows the density of the magnetic domains to be resolved locally. Furthermore the influence of the embossing is mapped globally by single sheet tests. The finite element analysis of the forming process derives the residual stress distribution which is responsible for the measured magnetic behavior. In order to isolate the influence of the residual stress, non-embossed and stress-relief annealed specimens are used as a reference for both measurement methods.

Keywords Electrical steel · Mechanical stress · Forming · Embossing · Production · Electric drives · Neutron grating · Single sheet tester

✉ Simon Vogt
simon.vogt@utg.de

Tobias Neuwirth
tobias.neuwirth@frm2.tum.de

Benedikt Schauerte
benedikt.schauerte@iem.rwth-aachen.de

Hannes Alois Weiss
hannes.weiss@utg.de

Peter Markus Falger
peter.falger@tum.de

Alex Gustschin
alex.gustschin@ph.tum.de

Michael Schulz
michael.schulz@frm2.tum.de

Kay Hameyer
post@iem.rwth-aachen.de

Wolfram Volk
wolfram.volk@utg.de

[1] Chair of Metal Forming and Casting, Technical University of Munich, Walther-Meißner-Str. 4, 85748 Garching, Germany

[2] Heinz Maier-Leibnitz Zentrum (MLZ), Technical University of Munich, Lichtenbergstr. 1, 85748 Garching, Germany

[3] Institute of Electrical Machines, RWTH Aachen University, Schinkelst. 4, 52062 Aachen, Germany

[4] Department of Physics and Munich School of Bioengineering, Chair of Biomediacal Physics, Technical University of Munich, James-Franck-Str. 1, 85748 Garching, Germany

1 Introduction

Mechanical stress and its influence on the magnetic properties of non-oriented electrical steels has generated high interest over the past years. Most of the investigations and publications on this topic are concentrated on the measurement, analysis and modeling of magnetic property and characteristic magnetic value deteriorations under dynamic loads caused by centrifugal forces [5, 8, 11, 12] and residual stress resulting from material processing such as blanking related effects [10, 13, 15]. Nevertheless, in addition to the obvious negative properties, the inverse magnetostrictive effect also offers the possibility of improving the operating behavior of rotating electrical machines by targeted manipulation of the material and by permitting a purposeful flux guidance as a result of targeted residual stress induced by embossing. In order to realize this and to enable a precise geometrical design of the non-oriented electrical steel laminations, an extended knowledge of the resulting residual stress distribution caused by embossing and a high-resolution analysis of their influence on the magnetic behavior is crucial. Neutron grating interferometry (nGI) allows a locally resolved measurement of the intrinsic stress distributions in non-oriented electrical steels resulting from embossings as well as insights about the domain density and thus the magnetization along the sheet metal cross-section.

This work aims to provide basic knowledge about the resulting residual stress distribution caused by the embossing process in non-oriented electrical steel and to establish its influence on the magnetic properties. For this purpose, samples of a commonly used silicon electrical steel were first embossed, then examined by nGI with regard to the resulting residual stress distribution and the domain density distribution under the influence of increasing magnetic field strengths and finally analyzed using a single sheet tester in order to depict the global effects of the residual stress.

2 Methods

2.1 Specimens

The geometry and manufacturing processes for sample preparation were chosen accordingly to the boundary conditions of the applied measurement methods. The maximum sample length for the magnetic yoke for the neutron grating interferometry (nGI) is 60 mm. In order to achieve a high flux density, the sample width was set to 10 mm. The single sheet tester has a measuring area of 60 mm × 60 mm, hence the measuring area is not completely filled with the selected sample geometry. Non-oriented electrical steel with a silicon content of 2.4% and a thickness of 0.35 mm as used in [13] was selected as the material to be tested.

To minimize the magnetic influence of cut edges, the samples are eroded as shown in Fig. 1. To ensure a reproducible position of the embossing in the sample, two locating holes were cut simultaneously with the embossing into the rectangular initial blank (dashed line). The locating holes were used to align the samples with pins while eroding. In order to maintain the positioning until the end of eroding, a bar with a width of 0.5 mm was maintained on each side of the specimen. In this condition, some of the specimens could be mounted on the holes for stress relief annealing. The stress relief annealing was carried out under inert gas (Argon 5.5) for 2 h at 700 °C. Finally, both parts at the end of the blank, containing the locating holes, were broken off and the remaining specimen was deburred.

The universal tool used has punches, aligned in a line with a spacing of 10 mm. It is possible to take punches out or change them in order to produce specimen with a different number of embossings. As already explained this allows the locating holes to be made at the same time as the embossing. To position two embossings in the middle of the blank, the specimen was eroded with an offset as shown in Fig. 1b. For the embossing a spherical punch with a diameter of 2.00 mm, a blank holder and a die with a diameter of 3.03 mm where used as shown in Fig. 2. The experiments were carried out on a Schuler stamping press CSP 100 with ServoDirect Technology.

The embossed geometry was 3D scanned with a Keyence VK-X100 Series Shape Measurement Laser Microscope. As shown in Fig. 3, the real embossing geometry can be digitized and the resulting embossing depth can be measured in

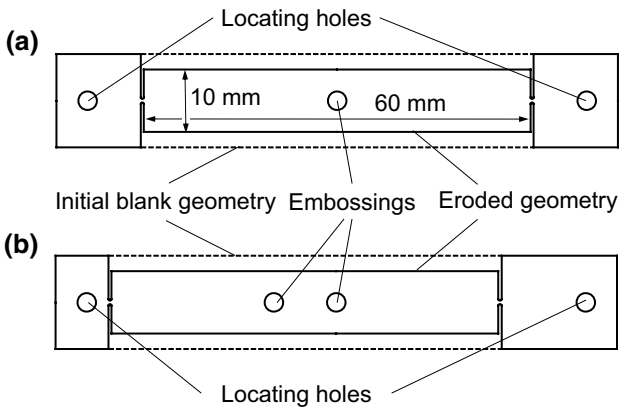

Fig. 1 Schematic illustration of the production of the specimens: **a** symmetric specimen with one embossing, **b** asymmetric specimen with two embossings

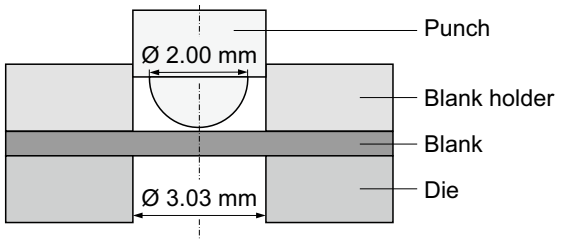

Fig. 2 Schematic illustration of the embossing tool. The used spherical punch had a diameter of 2.00 mm, the die had a diameter of 3.03 mm. A blank holder kept the blank in position

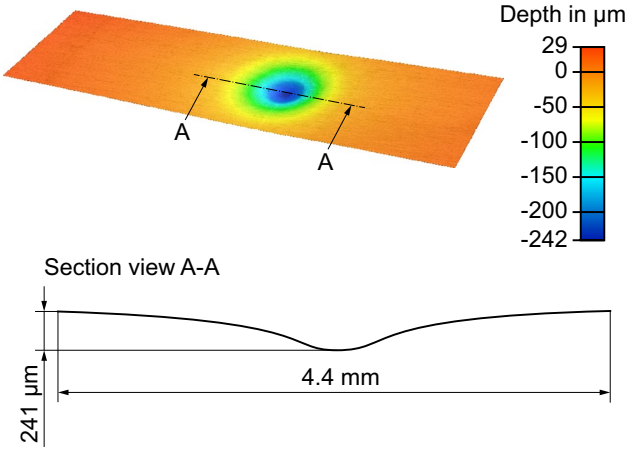

Fig. 3 3D scan and profile of the embossed sheet metal. The measured section view of the specimen indicates a maximum depth of 241 µm

the section view A–A. These data have been used to match the real embossed part in the FEA, which was used to calculate the residual stresses in the specimen.

2.2 Numerical methods

To understand the residual stress distribution within the specimens, the production process was modelled using finite element analysis (FEA). Therefore, a three dimensional setup was built up in Dassault Systems' Abaqus version 6.12-3. In order to get valuable results out of the FEA each step of the experimental embossing process has to be numerically modelled. These steps include clamping the electrical steel in between the blank holder and the die, embossing the electrical steel with a spherical punch and a final springback calculation of the embossed electrical steel.

In the first step the blank holder presses the electrical steel with a force of 25.5 kN onto the die. Afterwards, in the second step the punch penetrates the blank to an extent of 0.246 mm, which leads to elastic and plastic material deformations. Within the springback calculation, the punch and blank holder are removed from the electrical steel's surface, in order to be able to analyze the residual stress left in the material, respectively. The mentioned penetration depth was chosen in such a way, that the final numerical part geometry matches with the experimental one (Fig. 3). The first two steps are executed as an explicit dynamic analysis and the third step as an implicit static analysis.

As in the experimental setup, the punch is radially symmetric and it is centrally positioned towards die and blank holder. The sphere on the punch tip has a diameter of 2 mm. The die has a diameter of 3.03 mm. The die is assumed to have a sharp edge with a radius of 0.05 mm. As the embossing process is a symmetrical problem in two axes, just a quarter of it is simulated in order to reduce computation time.

The tools are analytically modelled as rigid bodies and the electrical steel sheet is meshed using 8-node linear brick C3D8R elements. Element edge size varies from 0.002 mm in zones exposed to high deformations to 2.5 mm in areas subjected to less deformation further away from the punch and the die. All together 37926 elements were used.

The anisotropic mechanical material properties determined in [13] are considered using a Hill'48 yield criterion. In addition strain rate dependent stress strain data is provided. Friction in between the tool parts and the electrical steel is implemented with a penalty contact and a friction coefficient of 0.14.

2.3 Evaluation methods

2.3.1 Neutron grating interferometry

Neutron grating interferometry (nGI) is a neutron imaging technique used to extract information about absorption, phase shift and ultra-small-angle scattering of neutrons (USANS) inside a sample. Especially the scattering image (DFI) generated by USANS is of high interest in mapping the local magnetic domain structure close to an embossing, as the neutrons are scattered off the magnetic domain walls, which are influenced by the applied stress and strain [2].

A neutron grating interferometer is a Talbot-Lau interferometer adapted to work with neutrons. The used grating interferometer consist of three line gratings, one of which is a phase grating (G_1), while the other two are absorption gratings (G_0 and G_2) [4].

Grating G_1 introduces a periodic phase modulation of π into the neutron wavefront, resulting in a split of the neutron wave into the first orders [9]. Due to this splitting of the neutron beam a complex intensity and phase modulation is observed behind G_1, which is called Talbot carpet [3]. The intensity modulation reaches a maximum at the odd fractional Talbot distances behind G_1. The Talbot carpet is

only generated if the incoming neutron beam has a certain spatial coherence.

To achieve this with a reasonable neutron flux the source grating G_0 is placed upstream of G_1, which splits the neutron beam in an array of coherent line sources, which are not coherent with respect to each other. At these distances, the resulting interference pattern has half the period of G_1. As this pattern is generally to small to be analyzed by neutron detectors, the analyzer (G_0) grating is needed [1]. Hence the analyzer grating, which hast the same period as the generated interference pattern, is placed at one of the odd fractional Talbot distances. By moving one of the gratings perpendicular to the grating lines, the interference pattern can be analyzed. Such a motion generates an intensity oscillation in every pixel of the neutron detector, from which the transmission image (TI), differential phase contrast image (DPCI) and the dark field image (DFI) are recovered.

The shown data has been acquired with the nGI-setup of the ANTARES imaging beamline at the FRM II. The measurements were performed at a correlation length of 1.865 µm. For each nGI-scan the G_1-grating was moved half its period, resulting in a movement of the interference pattern of one period. Three images were taken at each of the ten equidistant positions. Each image had an exposure time of 10 s, which resulted in a total exposure of 300s per nGI-scan. The effective pixel size was set to 27 µm × 27 µm, which resulted in a field of view of 70.3 mm × 83.3 mm. The used scintillation screen had a thickness of 100 µm. For each sample used, nGI-scans have been performed with different magnetic fields applied to map the resulting DFI-signal. The samples have been magnetized with a yoke as described in [14]. In Table 1 the applied currents and the resulting magnetic fields are shown.

2.3.2 Single sheet tests

The magnetic measurements of the embossed specimens are performed on a double joke single-sheet-tester (SST) which allows the standardized measurement of the magnetic properties of 60 mm × 60 mm specimens. The magnetic resistance of the two yokes which close the magnetic path can be neglected in comparison to the specimen due to the much wider cross-section of the two yokes in terms of the iron losses and the magnetic resistance. The magnetic field generated by electrical currents in the primary winding is controlled to cause a sinusoidal magnetic flux density of varying amplitudes and frequencies measured by the induced voltage in the secondary coil. The embossed 60 mm × 10 mm specimens are positioned in the middle of the double yokes and close to the magnetic circuit. The air flux compensation reduces the measured signal by the air flux B_0 which would also be present in air without a ferromagnetic material and ensures that solely the magnetic flux within the specimen is measured. Magnetic field and flux density are applied and measured parallel. The magnetic field is determined by means of the magnetic path length and the applied current in the primary winding. The magnetic flux density is measured by averaging the magnetic flux over the crosssection of the specimens. Thus, the deterioration of the materials magnetic properties can only be measured globally and not locally resolved.

Table 1 Applied currents and resulting magnetic fields

Current in A	0.00	0.47	1.34	2.00
Magnetic field in $\frac{A}{m}$	0.00	780	2230	3330
Current in A	3.00	4.00	5.00	6.67
Magnetic field in $\frac{A}{m}$	4995	6660	8330	11200

3 Results

3.1 FEA of residual stresses

In this section the results of the mechanical FEA are discussed. Since it is important to distinguish between tensile and compressive stress for their different extent on the magnetic material properties, no von Mises equivalent stress criterion can be used [7, 13]. Instead, the residual stress state within the embossed electrical steel is discussed regarding the local maximum absolute principle stress $\sigma_{\mathrm{max,principal,abs}}$.

The residual stress distribution of the embossed electrical steel is displayed in Fig. 4. Apart from the area within 5 mm around the embossing that is subjected to large stress, areas further away from the embossing are only subjected to tensile and compressive stress below 20 MPa. Due to the large spread of the induced residual stress, it is not possible

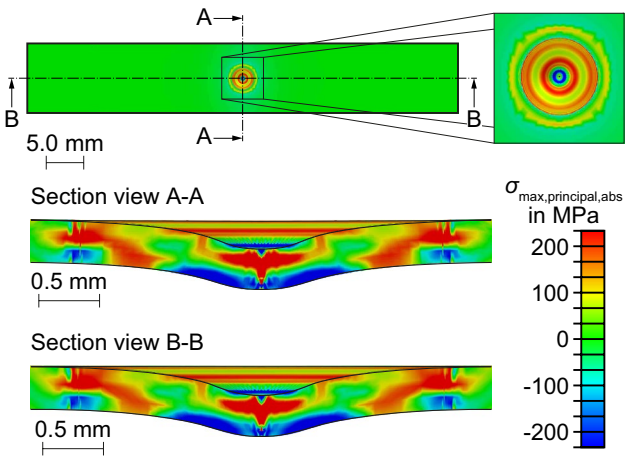

Fig. 4 Results of the FEA; specimen with embossing in detail, section view A–A of embossing and section view B–B of embossing

to visualize such small deviations. As the area subjected to larger stress around the embossing is quite small compared to the whole specimen, two section views A–A and B–B added within Fig. 4 allow for a detailed investigation of the embossing-related residual stress to be made.

As the two sections show, the anisotropic mechanical material properties do have a small but noteworthy influence on the effective residual stress state within the electrical steel. Local maximum principle stress values after embossing reach from −350 MPa for compression stress and up to 300 MPa for tension stress. Looking at the two section views, compressive stress is located mainly on the bottom side of the embossed electrical steel specimen, whereas tension stress is spread, outgoing from center, beyond the die diameter.

3.2 Neutron grating interferometry

To investigate the correlation between embossing and the local degradation of the magnetizability the DFI contrast is used. It has been shown that this contrast is directly correlated to the amount of domain walls present in a sample. Embossing causes internal stress which is locally applied to the electrical steel sheet. Due to the magneto elastic effect, this results in a increased domain wall density as well as in a decreased domain wall mobility, which results in a lower DFI signal. Hence, the DFI signal maps areas of increased internal stress. The embossed samples, annealed and non-annealed, were both normalized to their respective non-embossed samples. The embossing has been performed as described in Sect. 2.1.

The non-annealed sample (Fig. 5a) and the annealed sample (Fig. 5b) were both measured at the different magnetic fields as described in Sect. 2.3.1. For a magnetic field of 3330 $\frac{\mathrm{A}}{\mathrm{m}}$ the resulting normalized signals are shown in Fig. 5. It can be seen that for the non-annealed sample the signal near the embossed area, denoted by the red circle is below unity, indicating an increased magnetic domain density in the embossed sample compared to the non-embossed reference. In contrast, the signal of the annealed sample near the embossing is close to unity, indicating no change in the density of the magnetic domains compared to the non-embossed reference.

Hence, the change of the DFI signal is primarily caused by the stress and strain induced by embossing and not by the change of the geometry compared to a non-embossed electrical steel sheet. As already shown in the FEA, stress and strain are not confined to the contact area of the embossing tool, but also affect the surrounding material, which causes the increased magnetic domain density around the embossing area. The annealed sample shows only a small change of the DFI signal directly in the contact area between the spherical punch and the electrical steel. This change may be

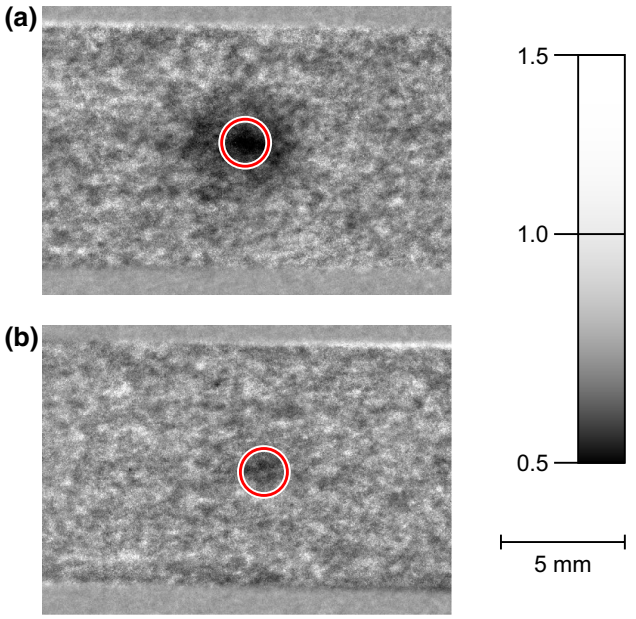

Fig. 5 Comparison of **a** an electrical steel sheet and **b** an annealed electrical steel sheet with an applied magnetic field of 3330 $\frac{\mathrm{A}}{\mathrm{m}}$. Both samples have been embossed with a spherical stamp and normalized to their respective non-embossed references. The location of the embossing in both samples is marked by the red circle. The diameter of the circle corresponds to the diameter (2 mm) of the sphere used as the stamp. While the annealed sample (**b**) shows nearly no signal change in the area of the embossing, the not annealed sample (**a**) shows a strong signal change around the area of the embossing

a result of the change in geometry, grain and hence domain structure due to the embossing. Alternatively, also some internal stress may remain after annealing, as the embossing depth is significant compared to the material thickness.

3.3 Single sheet tests

The magnetic properties of the embossed specimens can be measured with a conventional SST. By this means, the magnetizability of the specimens can be identified averaged over their cross section. For a first examination an unworked steel strip is compared to an embossed. The residual stress remains in the material due to the recesses are expected to increase the measured magnetic resistance as a result of the inverse magnetostrictive effect [6]. The magnitude of this deterioration of the magnetic behavior caused by the single flux barrier and with it its applicability for electrical machine design is to be determined thereby. To ensure that the deterioration of the magnetizability can be attributed to the residual stresses resulting from the embossing and not the geometric deformation of the material, the two samples are each compared with two annealed specimens in which very low residual stress should be present. The measurements were performed at sinusoidal magnetic flux

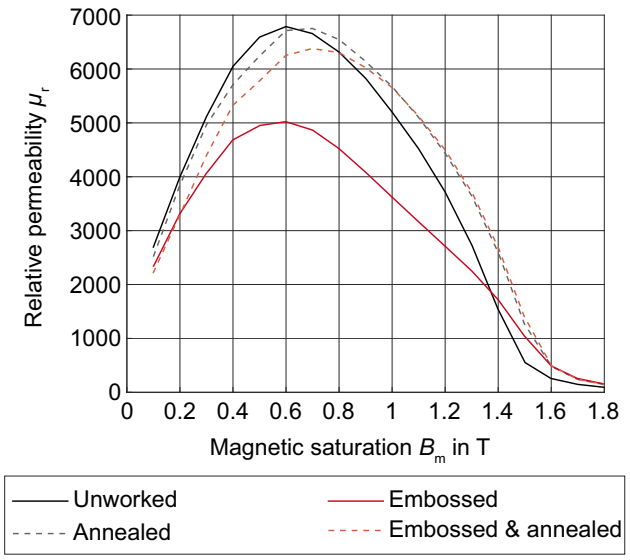

Fig. 6 Influence of embossing and annealing on relative permeability of examined non-oriented electrical steel sheets measured on 1D-SST

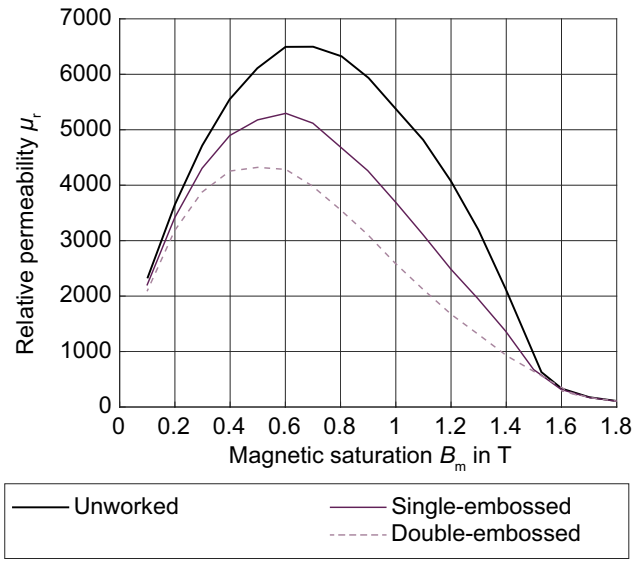

Fig. 7 Overlay effects of unworked, single and double embossed specimen on the magnetic permeability

densities rising from 0.1 up to 1.8 T with a frequency of 20 Hz. The criterion for the magnetisability of the specimens is the resulting magnetic permeability. In Fig. 6 the permeabilities of annealed and unfinished, embossed and original specimens measured at 20 Hz for rising peak inductions B_m and maximum magnetic field strengths H_m are compared. The two original geometries depicted in black show slight deviations. These deviations can be understood as a result of the residual stress due to the cutting of the 60 mm × 10 mm steel strips. As expected, the deformed specimen shows the lowest magnetic permeability of all specimens until a peak induction of 1.4 T is reached. For magnetic excitations below 1.4 T the magnetic permeability is reduced by almost 30%. The deformed specimen which was annealed subsequently to the deformation shows a clear improvement of the magnetization of the material. In regions over 1.0 T the curves are almost identical. At lower saturations the materials permeability is clearly below the non-deformed permeabilities, hence an influence of the sample geometry or remaining residual stress is still recognizable. Nonetheless the influence of the residual stresses turn out to be the main cause for the magnetic deterioration.

For later utilization of residual stress for the purposeful flux guidance an investigation of the behavior with several embossings in order to achieve larger flux barriers is desirable. In order to investigate whether the effects of several embossings superpose each other, samples with two subsequently embossings (see Fig. 1b) were prepared and magnetically characterized.

Figure 7 depicts the result of single and double embossed specimens versus the measurement of an unworked specimen. A correlation between the number of embossings and the deterioration of the magnetizability of the material is obvious. Below 1.4 T the decrease of the magnetic permeability is almost linear, while the peaks of the permeability moves towards weaker magnetic excitations B_m.

4 Conclusion

The residual stress for the selected specimen was determined by FEA. The use of neutron grating interferometry allows to locally resolve the changes in the magnetic flux caused by residual stress. The adapted single sheet test method also depicts the global influence of the residual stress introduced by embossing. Both methods were used to compare stress-relief annealed samples. These samples showed almost the same behavior as non-embossed samples. The influence of the number of embossings was demonstrated by means of single sheet tests. This confirms that the residual stress has a significant contribution to the guidance of the magnetic flux and that the shown measuring methods exclusively reflect the influence of residual stress.

Acknowledgements Funded by the Deutsche Forschungsgemeinschaft (DFG, German Research Foundation)—HA 4395/22-1; SCHU 3227/2-1; VO 1487/31-1.

References

1. Grünzweig C, Frei G, Lehmann E, Kühne G, David C (2007) Highly absorbing gadolinium test device to characterize the performance of neutron imaging detector systems. Rev Sci Instrum 78(5):053708. https://doi.org/10.1063/1.2736892

2. Grünzweig C, David C, Bunk O, Dierolf M, Frei G, Kühne G, Schäfer R, Pofahl S, Rønnow HMR, Pfeiffer F (2008) Bulk magnetic domain structures visualized by neutron dark-field imaging. Appl Phys Lett 93(11):112504. https://doi.org/10.1063/1.2975848
3. Hipp A, Willner M, Herzen J, Auweter S, Chabior M, Meiser J, Achterhold K, Mohr J, Pfeiffer F (2014) Energy-resolved visibility analysis of grating interferometers operated at polychromatic X-ray sources. Opt Express 22(25):30394–30409. https://doi.org/10.1364/OE.22.030394
4. Lau E (1948) Interference phenomenon on double gratings. Ann Phys 6:417. https://doi.org/10.1002/andp.19484370709
5. Leuning N, Steentjes S, Schulte M, Bleck W, Hameyer K (2016) Effect of elastic and plastic tensile mechanical loading on the magnetic properties of NGO electrical steel. J Magn Magn Mater 417:42–48
6. Leuning N, Steentjes S, Weiss HA, Volk W, Hameyer K (2018) Magnetic material deterioration of non-oriented electrical steels as a result of plastic deformation considering residual stress distribution. IEEE Trans Magn. https://doi.org/10.1109/TMAG.2018.2848365
7. Naumoski H, Maucher A, Herr U (2015) Investigation of the influence of global stresses and strains on the magnetic properties of electrical steels with varying alloying content and grain size. 5th Int Electric Drives Prod Conf (EDPC). https://doi.org/10.1109/EDPC.2015.7323206
8. von Pfingsten G, Hameyer K, Paul D (2016) Influence of axial mechanical stress on the magnetic properties of non-oriented electrical steel. In: 2016 6th international electric drives production conference (EDPC), 30 Nov–1 Dec 2016, IEEE, Nuremberg, Germany, pp 193–200. https://doi.org/10.1109/EDPC.2016.7851333
9. Reimann T (2017) Vortex matter beyond sans. PhD thesis, Technische Universität München
10. Saleem A, Alatawneh N, Chromik RR, Lowther DA (2016) Effect of shear cutting on microstructure and magnetic properties of non-oriented electrical steel. IEEE Trans Magn 52(5):1–4
11. Steentjes S, Rasilo P, Belahcen A, Kouhia R, Hameyer K (2016) Anisotropic model for Villari effect in non-oriented electrical steel sheets. In: Electromagnetic field computation (CEFC), 2016 IEEE conference on, IEEE, pp 1–1
12. Vandenbossche L, Jacobs S, Van Hoecke D, Attrazic E (2015) Impact of mechanical stresses on the magnetic performance of non-oriented electrical steels and its relation to electric machine efficiency. In: Transportation electrification conference and expo (ITEC), 2015 IEEE, IEEE, pp 1–6
13. Weiss H, Leuning N, Steentjes S, Hameyer K, Andorfer T, Jenner S, Volk W (2017) Influence of shear cutting parameters on the electromagnetic properties of non-oriented electrical steel sheets. J Magn Magn Mater 421:250–259
14. Weiss H, Steentjes S, Tröber P, Leuning N, Neuwirth T, Schulz M, Hameyer K, Golle R, Volk W (2018) Neutron grating interferometry investigation of punching-related local magnetic property deteriorations in electrical steels. J Magn Magn Mater. https://doi.org/10.1016/j.jmmm.2018.10.098
15. Weiss H, Tröber P, Golle R, Steentjes S, Leuning N, Elfgen S, Hameyer K, Volk W (2018) Impact of punching parameter variations on magnetic properties of non-grain oriented electrical steel. IEEE Trans Ind Appl. https://doi.org/10.1109/TIA.2018.2853133